Electronic Supplementary Material (ESI) for Materials Advances.

Supporting Information for

3D Printing Aqueous $Ti_3C_2T_X$ Inks for MXene-based Energy Devices

Mofetoluwa Fagade[a, +], Dhanush Patil[b, +], Sri Vaishnavi Thummalapalli[b], Sayli Jambhulkar[b], Dharneedar Ravichandran[b], Arunachala M. Kannan[c], and Kenan Song[d,*]

[a] Mechanical Engineering, The School for Engineering of Matter, Transport and Energy (SEMTE), Ira A. Fulton Schools of Engineering, Arizona State University, Tempe, AZ, USA 85281

[b] Systems Engineering, The School of Manufacturing Systems and Networks (MSN), Ira A. Fulton Schools of Engineering, Arizona State University (ASU), Mesa, AZ, USA 85212

[c] The Fuel Cell Laboratory, The Polytechnic School, Ira A. Fulton Schools of Engineering, Arizona State University, AZ USA, 85212

[d] Associate Professor of Mechanical Engineering at University of Georgia (UGA) and adjunct professor of Manufacturing Engineering, The School of Manufacturing Systems and Networks (MSN), Ira A. Fulton Schools of Engineering, Arizona State University, Mesa, AZ, USA 85212;

[+] Co-first authors

[*] Corresponding author, Email: kenan.song@uga.edu

Table of Contents

1. Synthesis of MAX phase:

Ti_3AlC_2 MAX phase was synthesized by crushing and cold-welding Titanium Carbide (TiC) (i.e., avg. particle size ~2 mm, 99.5 % purity), Aluminium (Al) (i.e., avg. particle size ~325 mesh, 99.5 % purity), and Titanium (Ti) (i.e., avg. particle size ~325 mesh, 99.5 % purity) in a 2:1.1:1 molar ratio.[1] All powders were purchased from Alfa Aesar. The milling process was carried out in a glovebox (VTI Universal, Gloucester, MA, U.S.) in an argon-purged environment to prevent oxidation of the elemental powders. The homogeneous mixture was sintered under a uniform argon flow in a tube furnace. The temperature was ramped at a rate of 5 °C/min to a maximum of 1350 °C, which was then maintained for 2 h. The loosely packed powders agglomerated and coalesced in the form of rigid, chalky flakes, which were crushed and sieved to form uniform Ti_3AlC_2 MAX phase powder (~38 µm particle size).

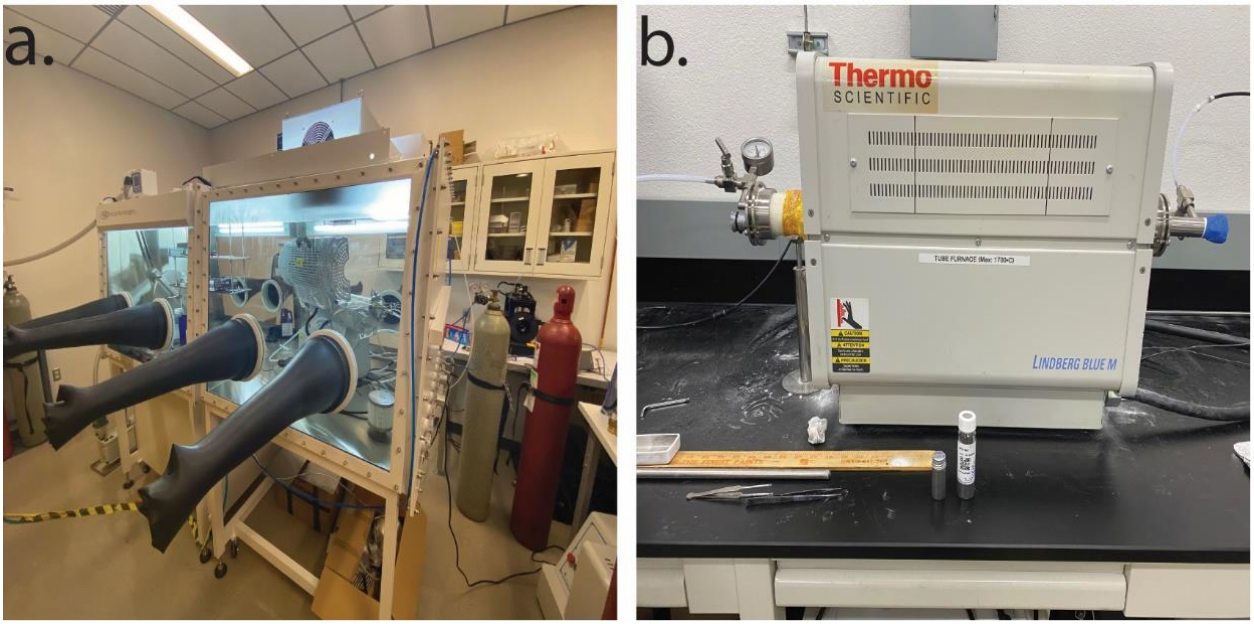

Figure S1. Experimental setup utilized for Ti_3AlC_2 synthesis. a) VTI Glovebox is employed to provide an inert environment (Argon gas kept at constant pressure) during the crushing and grinding of elemental powders (i.e., Titanium, Aluminum, and Titanium Carbide). b) ThermoScientific tube furnace used to carry out pressureless-sintering (PS)[2] of powders to produce the MAX phase. Temperatures reached a maximum of 1350 ^oC under constant argon flow.

2. Synthesis of MXenes:

$Ti_3C_2T_x$ MXene particles were derived from its Ti_3AlC_2 precursor using the in-situ HF etching method.[1,3] Before the etching, 74.7 mL of 12 M HCl was diluted in 100 mL of deionized (DI) water to form 9 M HCl. Then, 0.8 g of HCl was slowly added to 10 mL of 9 M HCl to avoid flashback from a resulting exothermic reaction. The solution was then magnetically stirred at a constant rate of 500 rpm for 10 min to create a homogeneous mixture.[1] Afterwards, 1 g of Ti_3AlC_2 was then gradually added to the premixed etchant mixture (i.e., LiF + HCl), and the mixture was stirred continuously for 24 h at a temperature of 35 °C and 500 rpm.[1] Once the etching was complete, the synthesized mixture was washed repeatedly with DI water until the pH of the supernatant reached a neutral value of ~6. The residue was then re-dispersed to form an aqueous colloidal solution. To delaminate the multi-layered $Ti_3C_2T_x$, the solution was then hand-shaken and centrifuged at 3500 rpm for 10 min.[1] Subsequently, a greenish-black stable dispersion formed, and the single-layer sheets were separated from their multi-layered counterparts, which settled at the bottom. The supernatant was then collected and vacuum-filtered through a PVDF membrane (i.e., 0.22 µm pore size, Durapore, Millipore) to form a thin film stored at low temperatures.

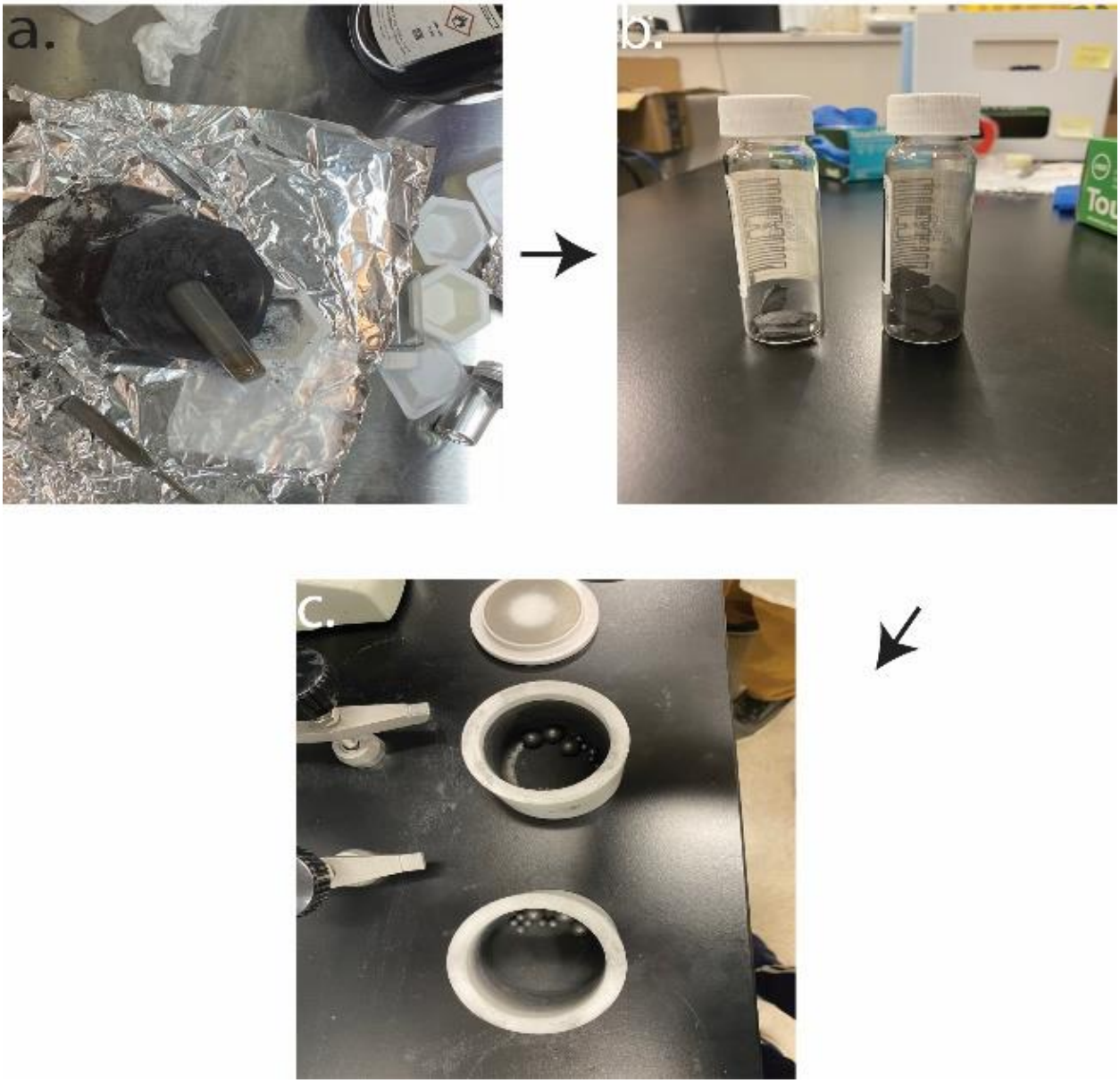

Figure S2. Different stages of MAX phase production. a) During grinding and cold welding in the glove box. b) Sintered Ti3AlC2 flakes after heat treatment. c) Ground powder after milling process in planetary ball mill.

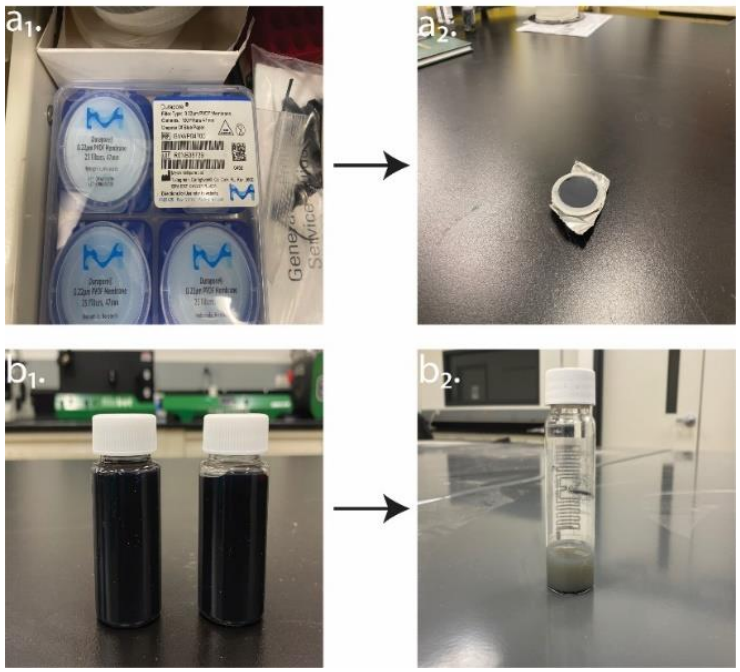

Figure S3. Distinct forms of MXenes were produced during the synthesis procedure. a_1) Filtration membrane used to produce the vacuum-assisted filtered film of MXene. a_2) Vacuum-assisted film of MXene. b_1) Aqueous colloidal $Ti_3C_2T_x$ ink solutions, which, when aged, decolorized to form b_2).

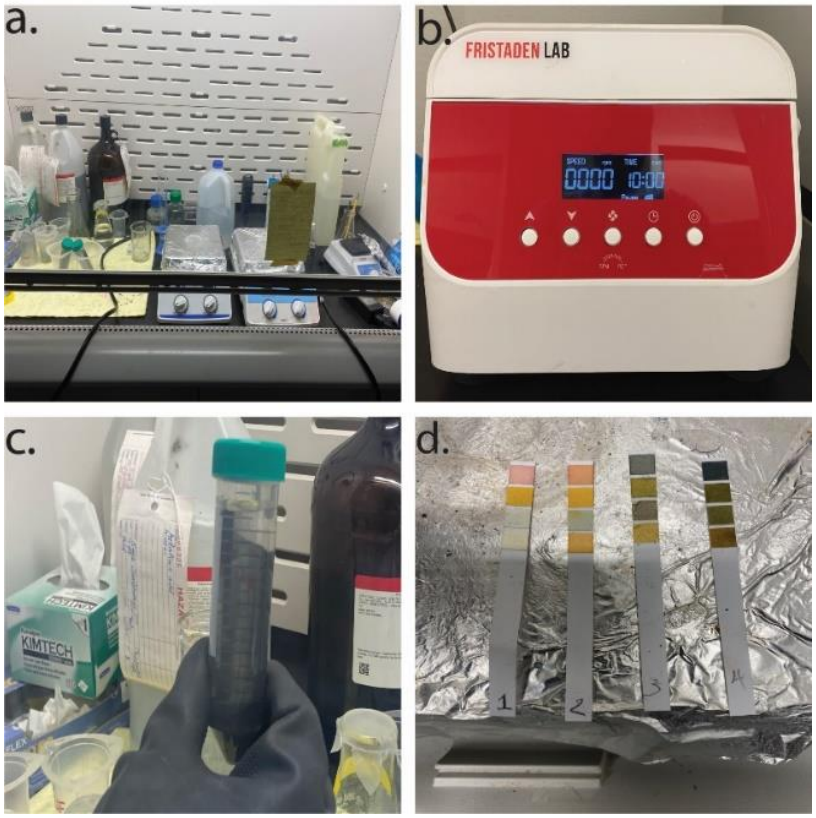

Figure S4. Experimental setup used to etch Ti_3AlC_2 and produce $Ti_3C_2T_x$. a) Fume hood containing LiF and HCl are utilized to create in-situ HF. b) Fristadenlab centrifuge used for washing cycles with DI water to reduce the pH of etched MXene. c) 30 mL vial containing $Ti_3C_2T_x$ slurry after a washing cycle. d) Litmus papers are used to analyze the pH of the aqueous solution after every washing cycle.

3. MAX and MXene Characterizations:

The microstructure and morphology of the MAX phase powders and MXene flakes were investigated using the scanning electron microscopy (SEM) (Zeiss Auriga) technique. Further analyses on the materials' internal phase structure and crystallography were performed using the X-ray diffraction (XRD) (PANalytical X'Pert PRO MRD) method. The spectra patterns were analyzed in an 8 - 70° (2θ) span. Tapping atomic force microscopy (AFM) (Witec Alpha 300 RA+) mode was utilized to visualize the surface topography of the delaminated MXene samples while providing high-resolution images (up to 0.5 nm).

4. Ink preparation and rheology:

4.1. Preparation of Aqueous $Ti_3C_2T_x$ Inks:

Isopropyl alcohol (IPA) and methylbenzene (toluene) were combined in the volumetric ratio (2.25:1) to form the antisolvent solution.[4] Then, the MXene/DI water slurry derived from post-washing cycles was added to the IPA/toluene solution. This was then centrifuged at 7800 rpm for 10 min and vacuum dried at room temperature until the solvent was evaporated entirely, leaving behind the sedimented MXene.[4] Later, this known amount of sediment was re-dispersed in DI water to obtain the required concentrations and sonicated for 8 h to create viscous $Ti_3C_2T_x$ ink.[4] This step was carried out to ensure the right concentration of MXene ink.

4.2. $Ti_3C_2T_x$ Ink Characterizations:

Rheology of the fabricated aqueous $Ti_3C_2T_x$ inks was performed on a Discovery HR-2 hybrid rheometer (TA Instruments, DE) with an 8 mm parallel plate, ETC Aluminum system (gap = 50 µm, amount ≈ 0.25 mL). The viscosity of the inks was then analyzed against the shear rate in the range of 0.1-1000 s^{-1}. The viscoelastic behavior constituting the elastic (G') and viscous (G") moduli of the MXene dispersion have been determined as a function of angular frequency in the range of 0.1 – 100 rad/s at a constant strain % of 1.0 %.

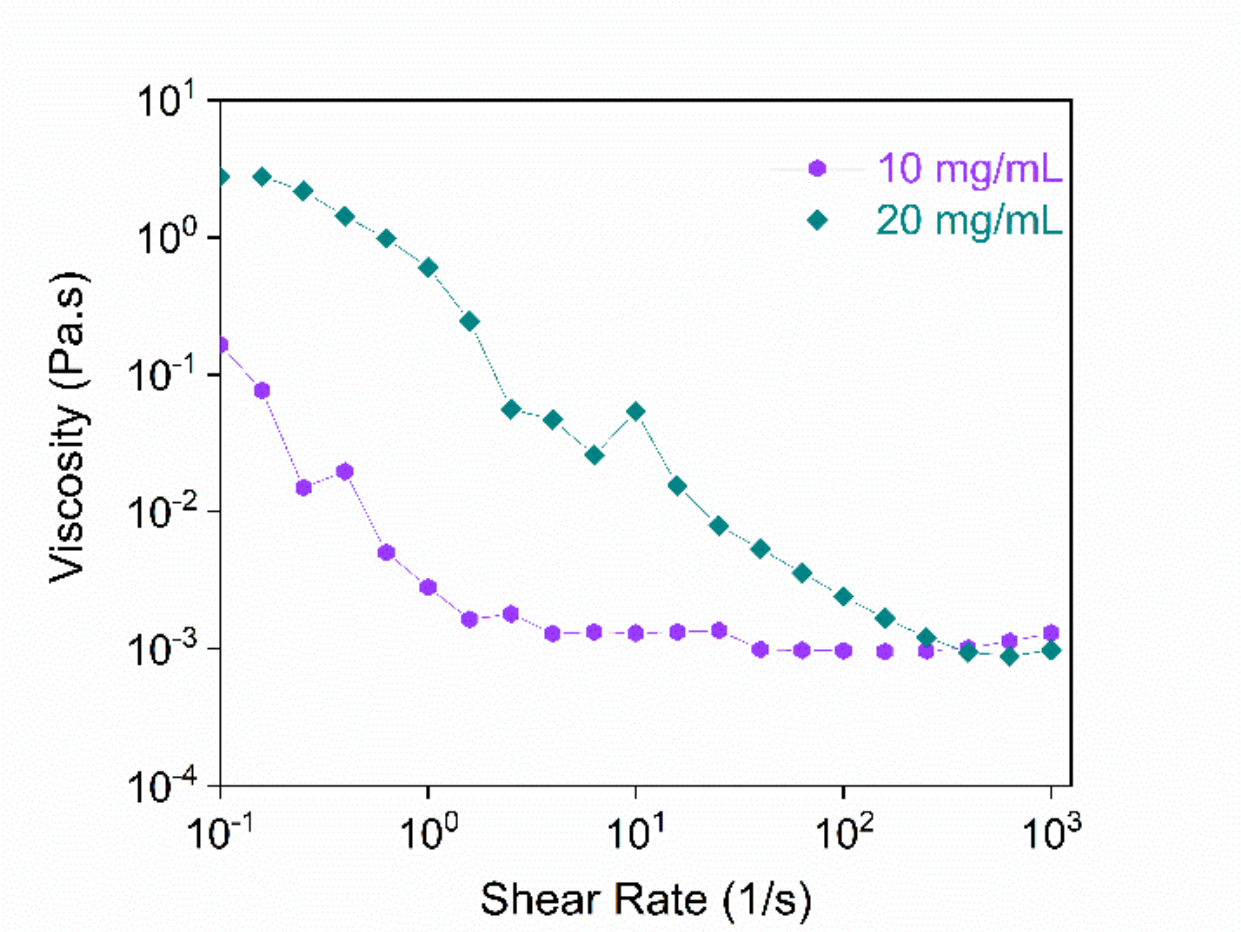

Figure S5. Flow sweep rheology analyzing viscosity behavior with the increasing shear rate for the low-concentration inks

5. Direct Ink Writing of $Ti_3C_2T_x$ Inks:

A Hyrel 3D Hydra system was utilized for direct ink writing (DIW) of the ink solutions (i.e., 100 mg mL^{-1} and 200 mg mL^{-1}). The aqueous dispersions were loaded into a 10-cc syringe (AHS, USA) and attached to a motorized fluid dispensing pump system (KD Scientific LEGATO 200). The pulse was set at a rate of 0.075 mL min^{-1}, and $Ti_3C_2T_x$ ink was used to form various (e.g., straight line or zigzag) surface patterns.

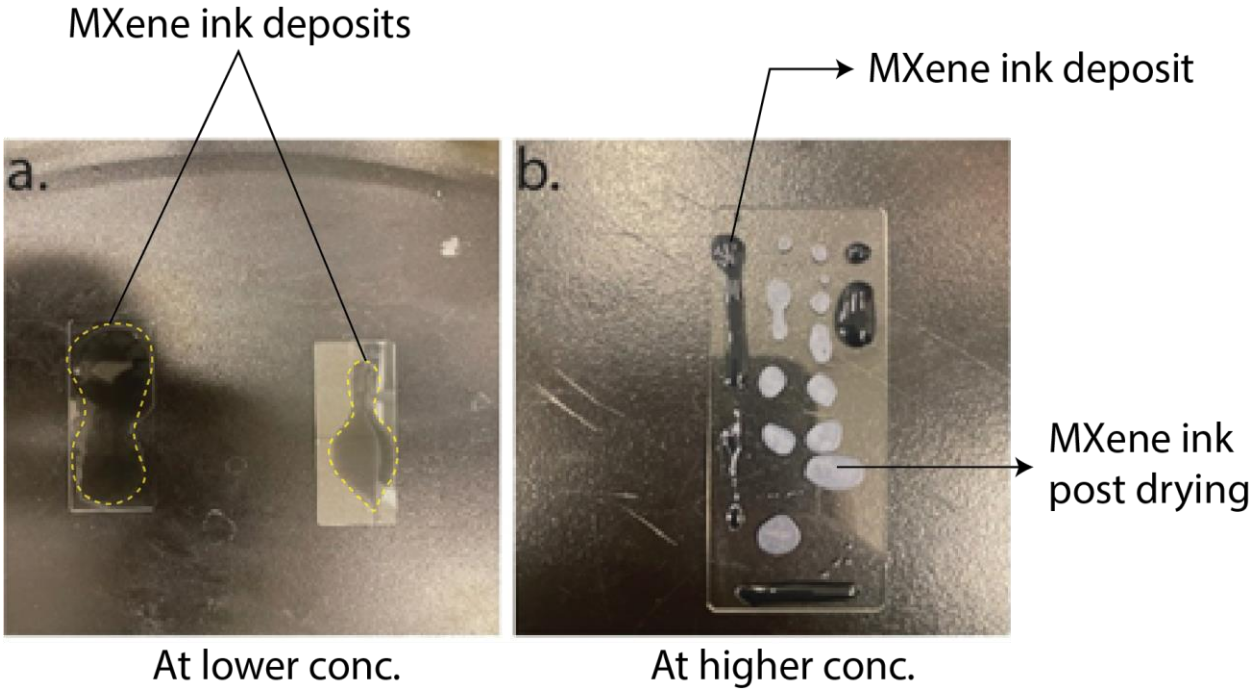

Figure S6. Early trials analyze the effects of parameters on flow behavior. a) Initial deposition on a glass substrate with 10 mg mL^{-1} aqueous MXene solution. b) Improved deposition on a glass substrate with higher concentrations of $Ti_3C_2T_x$ content.

6. Electrical performance of $Ti_3C_2T_x$:

6.1. A comparison of the electrical conductivity across various examples of MXene inks.

MXene ink	Concentration	Conductivity (S/cm)	Fabrication method	Post-processing	Reference
Aqueous-$Ti_3C_2T_x$	22.4 mg/mL	450	Inkjet printing		6
Ti3C2Tx – in – Water	30 mg/mL	10	Inkjet printing	Dried @ RT	7
$Ti_3C_2T_x$/ODA	20 mg/mL	8.74	Extrusion 3D printing	Annealing	8
$Ti_3C_2T_x$/AlOOH	104.6 mg/mL	532.3	Extrusion 3D printing	Freeze drying	9
Aqueous-$Ti_3C_2T_x$/PH1000	30 mg/mL	615	Inkjet printing		10
Aqueous-$Ti_3C_2T_x$	50 mg/mL		Extrusion 3D printing	Freeze drying	11
Aqueous-MXene/rGO	70 % (MXene loading)	1013	Extrusion 3D printing	Freese drying, Annealing	12
PEDOT: PSS/ $Ti_3C_2T_x$	120 mg/mL	1073	Extrusion 3D printing	Freezing 3D printing	13
HA-5/Alg-1/Ti_3C_2	1 mg/mL 5 mg/mL	0.0055 0.0072	Extrusion 3D printing	Crosslinking ($CaCl_2$)	14
Aqueous Ti_3C_2Tx	300 mg/mL		Extrusion 3D printing	Freeze-dried	15
TOCNFs/Ti3C2-50%	50 %	2.11	Extrusion 3D printing	Ethanol coagulation (solvent exchange)	16
Ti_3C_2/PEDOT: PSS	80 % Pure	1600 4000	Extrusion 3D printing	Dried overnight @ 60°C	17
Aqueous-$Ti_3C_2T_x$	100 mg/mL	1500	Extrusion 3D printing	Drying @ RT	This work

Table S1. Compares the electrical conductivities of different MXene-based inks concerning their concentration.

6.2. MXene-based Interdigitated Capacitor.

The 100 mg mL^{-1} MXene ink was deposited on PVA coated glass slide to fabricate the test samples for capacitive sensing. Later, copper wires formed connections, realizing an interdigitated capacitor setup. The sample was then encapsulated in PVA again before being peeled off. The copper wire terminals of the capacitor were connected to the terminals of the KEITHLEY DMM7510 7 ½ DIGIT MULTIMETER, using which the capacitance was measured. Input parameters were tap, tap and hold corresponding to short and long instance responses to finger touch.

6.3. Change in resistance with increasing strain.

A similar sample (100 mg mL^{-1}), as mentioned in section 6.2, was prepared, but with zig-zag patterns such that the conductivity wouldn't be affected at increasing strain due to the close-to serpentine pattern. The sample was clamped onto the TA Instruments Discovery HR-2's tensile setup. In-situ resistance was measured using the KEITHLEY DMM7510 7 ½ DIGIT MULTIMETER. Tensile loading was programmed at a linear rate of 2 µm s^{-1} corresponding to 0.01 – 5 % strain.

7. The stretchability of the device:

The printed patterns were sandwiched between PDMS for the MXene-based printed pattern to be sustainable for twisting and bending. Since PDMS is an elastomer, it has good elasticity, which makes the device conform to mechanical deformation, making it a good candidate for stretchable sensing.

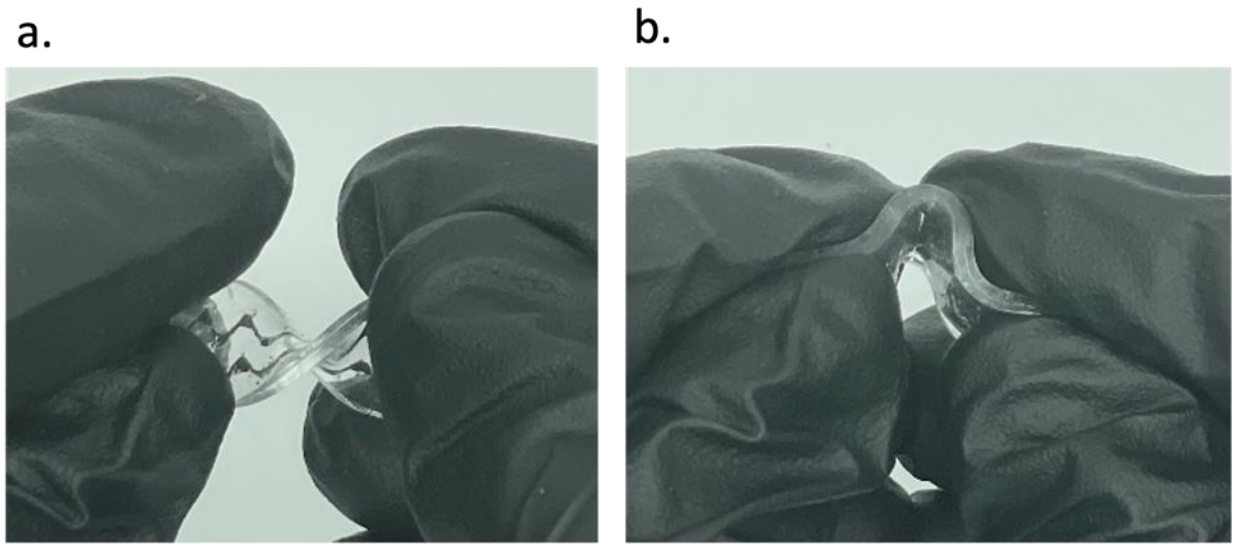

Figure S7. a&b) The printed MXene pattern encapsulated in PDMS is twisted and bent to show stretchability.

8. Electrochemical Characterization of $Ti_3C_2T_x$ Coated Electrode:

A three-electrode cell was designed to conduct the electrochemical test. The MXene ($Ti_3C_2T_x$) was employed as the working electrode, Saturated Calomel Electrode (SCE) was utilized as the counter electrode, and a platinum wire was used as the reference electrode.[5] Aqueous alkaline 1 M KOH solution was the electrolyte selected for this test. Furthermore, the CV measurements were analyzed using a Parstat 2273 electrochemical system at multiple scan rates (i.e., 10, 25, 75, and 100 mV s^{-1}) in the potential window (-0.7 to 0.7 V). The test setup was stabilized at a 50 mV s^{-1} scan rate for 20 cycles. Once stabilized, the sample was run at varying scan rates, each getting two cycles.

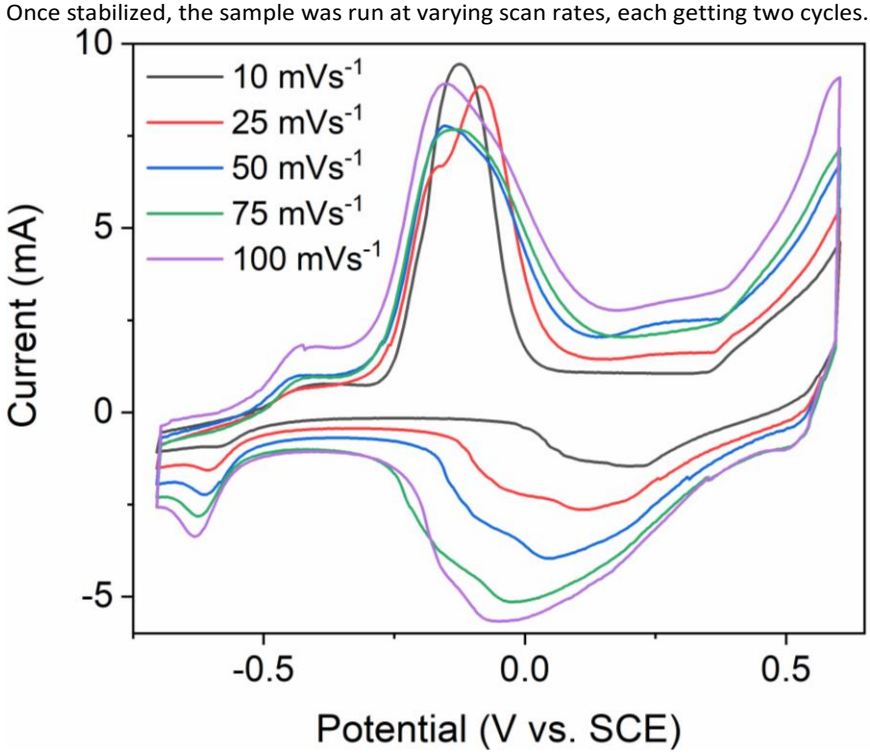

Figure S8. Cyclic Voltammetry of MXene Ti3C2Tx run at different scan rates (10, 25, 50, 75, 100 mVs-1) within the potential window of -0.7 V to +0.7 V.

A set of cyclic voltammetry (CV) tests was performed to observe the electrochemical behavior of the MXene ink solution. To create a rough surface morphology that facilitates ink deposition and prevents agglomeration of the MXene nanoparticles, a copper electrode was polished with sandpaper and sonicated in soap solution for about 8 hours. The electrode was then cleaned to remove impurities that could affect the experiment's accuracy. A three-electrode system used the MXene-coated electrode to produce the anodic and cathodic peaks (**Figure** S9). Different scan rates (10, 25, 75, and 100 mV s^{-1}) were used in the experiment, with the integral area increasing as the scan rate increased. Additionally, the current density held by the electrode increased at higher scan rates.

The charge storage mechanism of the fabricated electrodes was then observed from cyclic voltammetry (CV) studies. The CV curves show the presence of anodic and cathodic peaks for MXene particles. The increase in integral area concerning the scan rate indicates the redox peaks slightly shift indicating the lower potential. At high scan rates such as 100 mV s^{-1}, the ions migration into electrode materials becomes arduous, and less diffusion occurs, resulting in the deviation of the CV shape. The increase in scan rate increases the current density. However, the electrode material's specific capacitance (C_{sp}) value is decreased. The specific capacitance values were calculated from the CV curves.

$$C_{sp} = \frac{\int IdV}{vm\Delta V} \quad (1)$$

Where Csp is specific capacitance (F g^{-1}), 'I' stands for current (A), ∫Idv is the integral area under the CV curve, 'v' is the scan rate, ΔV is the change in voltage, and 'm' is the active mass loaded on the electrode, respectively. Although the integral area for the 100 mV s^{-1} scan rate is the largest, the lower scan rate (10 mVs-1) possesses the highest specific capacitance of 17.15 F g^{-1} compared to 4.36 F g^{-1} at 100 mV s^{-1}.

References

1 S. Jambhulkar, S. Liu, P. Vala, W. Xu, D. Ravichandran, Y. Zhu, K. Bi, Q. Nian, X. Chen and K. Song, *ACS Nano*, 2021, **15**, 12057–12068.

2 K. Lu, *International Materials Reviews*, 2008, **53**, 21–38.

3 W. Y. Chen, X. Jiang, S.-N. Lai, D. Peroulis and L. Stanciu, *Nat Commun*, 2020, **11**, 1302.

4 S.-H. Seok, S. Choo, J. Kwak, H. Ju, J.-H. Han, W.-S. Kang, J. Lee, S.-Y. Kim, D. H. Lee, J. Lee, J. Wang, S. Song, W. Jo, B. M. Jung, H. G. Chae, J. S. Son and S.-Y. Kwon, *Nanoscale Adv*, 2021, **3**, 517–527.

5 Y. Zhang, Z. Zhao, C. Luo, X. Wu and W. Chen, *Appl Surf Sci*, 2022, **578**, 152030.

6 S. Uzun, M. Schelling, K. Hantanasirisakul, T. S. Mathis, R. Askeland, G. Dion and Y. Gogotsi, *Small*, 2021, **17**, 2006376.

7 E. Quain, T. S. Mathis, N. Kurra, K. Maleski, K. L. Van Aken, M. Alhabeb, H. N. Alshareef and Y. Gogotsi, *Adv Mater Technol*, 2019, **4**, 1800256.

8 L. Li, Z. Deng, M. Chen, Z.-Z. Yu, T. P. Russell and H.-B. Zhang, *Nano Lett*, 2023, **23**, 155–162.

9 X. Wu, T. Tu, Y. Dai, P. Tang, Y. Zhang, Z. Deng, L. Li, H.-B. Zhang and Z.-Z. Yu, *Nanomicro Lett*, 2021, **13**, 148.

10 J. Ma, S. Zheng, Y. Cao, Y. Zhu, P. Das, H. Wang, Y. Liu, J. Wang, L. Chi, S. (Frank) Liu and Z. Wu, *Adv Energy Mater*, 2021, **11**, 2100746.

11 W. Yang, J. Yang, J. J. Byun, F. P. Moissinac, J. Xu, S. J. Haigh, M. Domingos, M. A. Bissett, R. A. W. Dryfe and S. Barg, *Advanced Materials*, 2019, **31**, 1902725.

12 Y. Dai, X. Wu, L. Li, Y. Zhang, Z. Deng, Z.-Z. Yu and H.-B. Zhang, *J Mater Chem A Mater*, 2022, **10**, 11375–11385.

13 L. Li, J. Meng, X. Bao, Y. Huang, X. Yan, H. Qian, C. Zhang and T. Liu, *Adv Energy Mater*, 2023, **13**, 2203683.

14 H. Rastin, B. Zhang, A. Mazinani, K. Hassan, J. Bi, T. T. Tung and D. Losic, *Nanoscale*, 2020, **12**, 16069–16080.

15 K. Shen, B. Li and S. Yang, *Energy Storage Mater*, 2020, **24**, 670–675.

16 W. Cao, C. Ma, D. Mao, J. Zhang, M. Ma and F. Chen, *Adv Funct Mater*, 2019, **29**, 1905898.

17 A. Ghaffarkhah, M. Kamkar, Z. A. Dijvejin, H. Riazi, S. Ghaderi, K. Golovin, M. Soroush and M. Arjmand, *Carbon N Y*, 2022, **191**, 277–289.